AGU PUBLICATIONS

JGR

Journal of Geophysical Research: Atmospheres

RESEARCH ARTICLE

10.1002/2014JD021749

Key Points:

- D-vortex merger is modulated by more intense African easterly waves
- The D-vortex merger occurred in 70% of Atlantic TCs formed in the MDR
- Average intensity of wet vortices is significantly more intense for DM than NM

Correspondence to:
S.-H. Chen,
shachen@ucdavis.edu

Citation:
Chen, S.-H., and Y.-C. Liu (2014), The relation between dry vortex merger and tropical cyclone genesis over the Atlantic Ocean, *J. Geophys. Res. Atmos.*, *119*, 11,641–11,661, doi:10.1002/2014JD021749.

Received 10 MAR 2014
Accepted 29 SEP 2014
Accepted article online 1 OCT 2014
Published online 28 OCT 2014

The relation between dry vortex merger and tropical cyclone genesis over the Atlantic Ocean

Shu-Hua Chen[1] and Yi-Chin Liu[1,2]

[1]Department of Land, Air, and Water Resources, University of California, Davis, California, USA, [2]Pacific Northwest National Laboratory, Richland, Washington, USA

Abstract Using 33 year European Centre for Medium-Range Weather Forecasts Re-Analysis Interim reanalysis in the months of August and September, we found that more than half of the low-level, moist vortices (called wet vortices) originating from south of the African easterly jet merged with a shallow, dry vortex from the north after leaving the West African coast. A dry vortex involved with the merger process is referred to as a D-vortex, and the process is referred to as a D-vortex merger. Dry vortices influenced by more intense African easterly waves moved southwestward and had a greater potential to serve as D-vortices in the merger process. The D-vortex merger occurred in the predepression stage of 70% of tropical cyclones (TCs) that formed in the Atlantic main development region and in 55% of nondeveloping systems. Further analysis showed that developing systems with the D-vortex merger (DM) were statistically dominated by a more intense wet vortex whose 500 hPa relative humidity was also significantly higher, while nondeveloping systems with the D-vortex merger (NM) were dominated by a more intense dry vortex. The average intensity of wet vortices for DM was more intense than that for NM, significant at a 95% confidence level. Moreover, warmer Saharan air was observed for DM than NM. While TC genesis is largely controlled by the large-scale environment over ocean, differences in vortex characteristics and environment over northwestern Africa between DM and NM could potentially help predict whether a tropical system associated with the D-vortex merger will ultimately evolve into an Atlantic TC.

1. Introduction

Previous studies have shown a high correlation between the occurrence of tropical cyclones (TCs) (A list of acronyms that are used in this study is provided in Appendix A) over the Atlantic Ocean and tropical waves originating from Africa. About 62% of tropical depressions [*Avila et al*., 2000] and more than 80% of intense hurricanes [*Landsea*, 1993] over the Atlantic Ocean developed from African tropical waves. However, while an average of 61 African tropical waves are produced each year, only 18% of them develop into tropical depressions [*Avila et al*., 2000]. While many key ingredients for TC genesis have been identified since *Gray* [1968], the key mechanisms that stimulate TC genesis for such a small fraction of African tropical waves still remind unclear.

Several environmental conditions have long been recognized as being favorable for TC genesis. These include weak vertical wind shear, high moisture content in low and middle levels, large positive relative vorticity in low levels at initial formation, and warm sea surface temperature [*Gray*, 1968]. Scientists have used this knowledge to develop empirical indices to help predict TC genesis. *Emanuel and Nolan* [2004] developed a TC genesis potential (GP) index, which is computed using four environmental parameters: 850 hPa absolute vorticity, 700 hPa relative humidity, potential intensity which is a function of sea surface temperature, and vertical wind shear. Several studies have investigated the applicability of the GP and suggested modifications to further improve TC genesis forecasting [*Emanuel*, 2010; *Tippett et al*., 2011; *McGauley and Nolan*, 2011]. *Bruyere et al*. [2012], for instance, removed absolute vorticity and relative humidity from the GP to produce a revised index, known as the cyclone genesis index (CGI), which they claimed better captured the seasonal and interannual variability of TC genesis over the North Atlantic Ocean.

Using 6 years of analysis data, *Peng et al*. [2012] revisited the environmental parameters that control TC genesis over the North Atlantic Ocean and concluded that the three most important parameters are the 925–400 hPa column-integrated water vapor content, rain rate, and sea surface temperature, all of which are thermodynamic variables. If disturbances only in the eastern Atlantic Ocean were considered, 700 hPa relative vorticity replaced rain rate as one of the three important parameters. Their findings are quite distinct from those used in the GP or CGI.

As TCs are multiscale phenomena, the role of mesoscale vortices and convective clouds in TC genesis can be substantial. *Berry and Thorncroft* [2005] showed that the rapid cyclogenesis of Hurricane Alberto resulted from a strong potential vorticity (PV) vortex that developed after two separate PV maxima merged just off the West African coast. One of these maxima was embedded within an African easterly wave (AEW) at 700 hPa, while the other low-level maximum was associated with a convective system, an African tropical wave, over the Guinea Highlands. *Karyampudi and Pierce* [2002] also found that tropical storm Ernesto (1994) and Hurricane Luis (1995) developed from the merging of 925 hPa and 700 hPa vortices over the eastern Atlantic Ocean. *Ross and Krishnamurti* [2007] revealed another vortex merger process between a moist low-level vortex associated with a convective African tropical wave to the south of the African easterly jet (AEJ) and a shallow dry vortex to the north of the jet. They linked cases where this merging process occurred to the genesis of specific TCs over the eastern Atlantic Ocean. This merging process is the focus of this study.

For simplicity, we define a "wet vortex" to be a low-level convective vortex along the West African coast to the south of the AEJ, while we define a "dry vortex" to be a dry, warm vortex near the West African coast to the north of the AEJ. Note that the wet vortices in this study are same as the southern vortices defined in *Pytharoulis and Thorncroft* [1999], while the dry vortices include both the northern vortices defined in the 1999 study and vortices that are shed from a vortex strip located in northwestern Africa (more discussion in section 3). In order to differentiate merger dry vortices from nonmerger dry vortices, we name the dry vortex that is involved in the merger process a "D-vortex," a term unique to this study. Note that a D-vortex is always a dry vortex, but not vice versa.

Since there is no universal TC genesis parameter, which suggests that the physical processes leading to genesis are not yet well understood, identifying physical processes that may improve TC genesis forecasting continues to be an important task. In this study, analyses from a 33 year data set (1980–2012 for August and September) showed that the D-vortex merger, in addition to the characteristics of the associated vortices and their environment, might play an important role in or serve as a predictor of TC genesis over the Atlantic Ocean. This study investigates the relation of the D-vortex merger to TC genesis over the Atlantic Ocean based on statistical analysis using the European Centre for Medium-Range Weather Forecasts Re-Analysis Interim data set. The ultimate goal of this study is to provide another potential parameter for TC genesis forecasting based on the D-vortex merger process.

This paper is organized as follows: in section 2 a case study of Tropical Storm Debby (2006) is used to illustrate the D-vortex merger process, introducing the fundamental physics underlying the vortex merger. In section 3, the sources of D-vortices are explored. The relationship between D-vortex merger events, African tropical disturbances, vortex characteristics, and vortex environmental conditions are investigated in section 4. Summary and conclusions are given in section 5.

2. The D-Vortex Merger

The European Centre for Medium-Range Weather Forecasts Re-Analysis Interim (ERAI) data set, which has a grid spacing of about 0.7° × 0.7°, was used for the present analysis. Since the D-vortex is from the north and is associated with air from the Saharan desert, we define a Saharan air parameter to describe the warmth and dryness of the desert air:

$$\mathrm{SAP} = \begin{cases} \left(\theta\text{-}\overline{\theta}\right)\times \mathrm{Rh_{dep}}, & \text{if } \theta > \overline{\theta} \text{ and } \mathrm{Rh_{dep}} > 0 \\ 0, & \text{otherwise} \end{cases}$$

where θ, $\overline{\theta}$, and $\mathrm{Rh_{dep}}$ are the 900 hPa potential temperature, mean potential temperature within 50°W–50°E and 0–40°N, and relative humidity (RH) depression, respectively. In this study, RH depression is defined as $\mathrm{Rh_{dep}} = (40\% - \mathrm{RH})$. The 900 hPa pressure level was chosen because we found that warm, dry air penetrates farthest south at the 900 hPa level, and the use of RH = 40% reasonably defines the spatial extent of dry Saharan air, as determined by examining the reanalysis data during our study period.

2.1. Tropical Storm Debby (2006)

Tropical Storm Debby (2006) was one of seven waves observed during the National Aeronautics and Space Administration (NASA) African Monsoon Multidisciplinary Analyses field campaign [*Zawislak and Zipser*, 2010]. Debby developed from a mesoscale convective system (MCS) that started organizing at 0000 UTC on

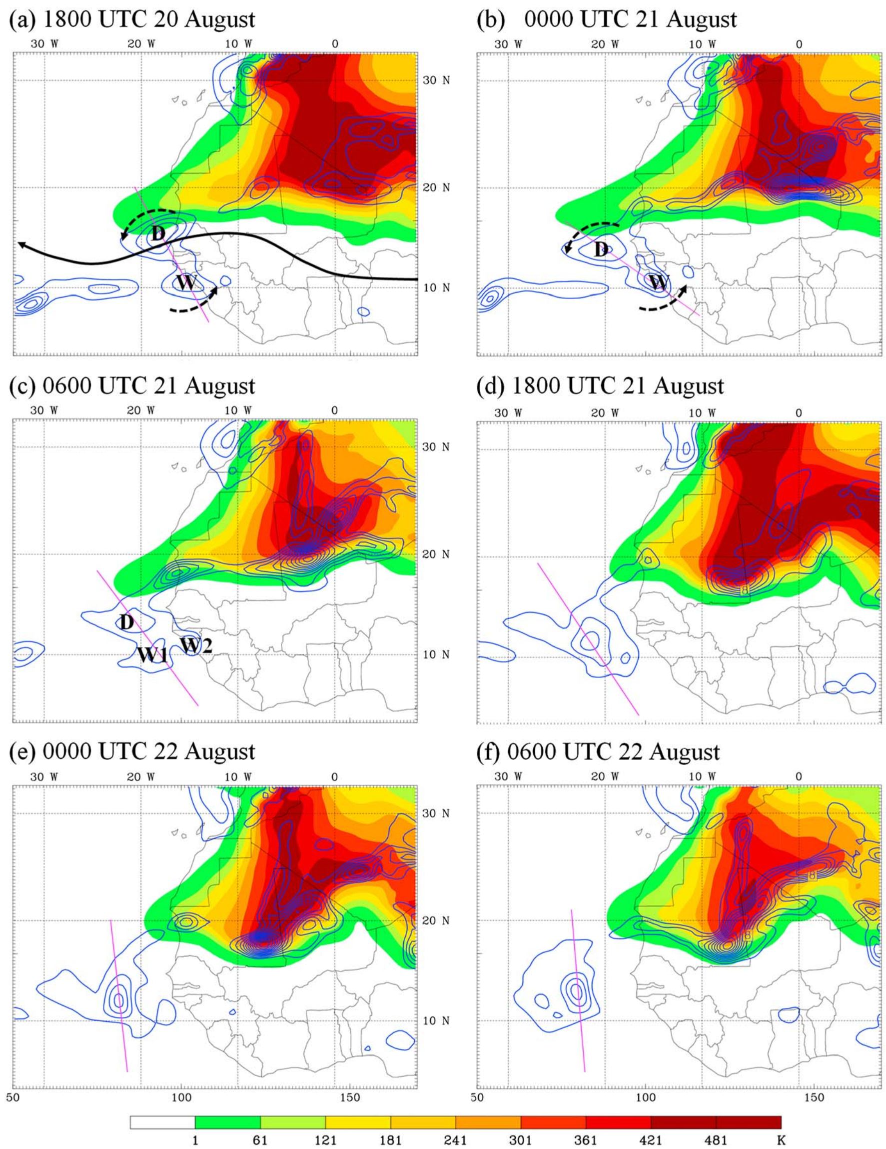

Figure 1. The 900 hPa positive relative vorticity (blue contour lines, 10^{-5} s^{-1}) and Saharan air parameter (SAP; shading; K) at (a) 1800 UTC on 20 August, (b) 0000 UTC on 21 August, (c) 0600 UTC on 21 August, (d) 1800 UTC on 21 August, (e) 0000 UTC on 22 August, and (f) 0600 UTC on 22 August 2006 from the ERAI data. The black solid arrow in Figure 1a indicates the position of the 700 hPa African easterly jet. The position of the AEJ was depicted by following the 700 hPa maximum wind speed along the AEJ at 1800 UTC on 20 August. The black dashed lines denote the clockwise rotation of the two vortices. The magenta lines in Figures 1a to 1f indicate the locations of the vertical cross sections for Figures 3a to 3f, respectively. The letters W and D indicate the wet vortex and D-vortex, respectively. W1 and W2 in Figure 1c indicate two vortices that split from the wet vortex (W).

18 August 2006 after moving south of Niger. The convective system became disorganized while crossing the West African highlands before reorganizing again over the ocean at 0000 UTC on 21 August. It was first classified as a tropical depression at 1800 UTC on 21 August before beginning to move northwestward. Debby was later classified as a tropical storm at 0000 UTC on 23 August but never developed into a hurricane.

According to the tropical cyclone report from the National Hurricane Center Debby's genesis was rather rapid and relatively difficult to predict. In fact, its genesis was predicted only 3 h in advance. Because of this, Debby has received a considerable amount of attention from researchers, particularly in the investigation of its genesis and development [*Jenkins et al*., 2008; *Zipser et al*., 2009; *Vizy and Cook*, 2009; *Sippel et al*., 2011; *Ventrice et al*., 2012]. We found that Debby's predepression system was involved with the D-vortex merger after leaving the West African coast and decided to use it to demonstrate the D-vortex merger process.

10.1002/2014JD021749

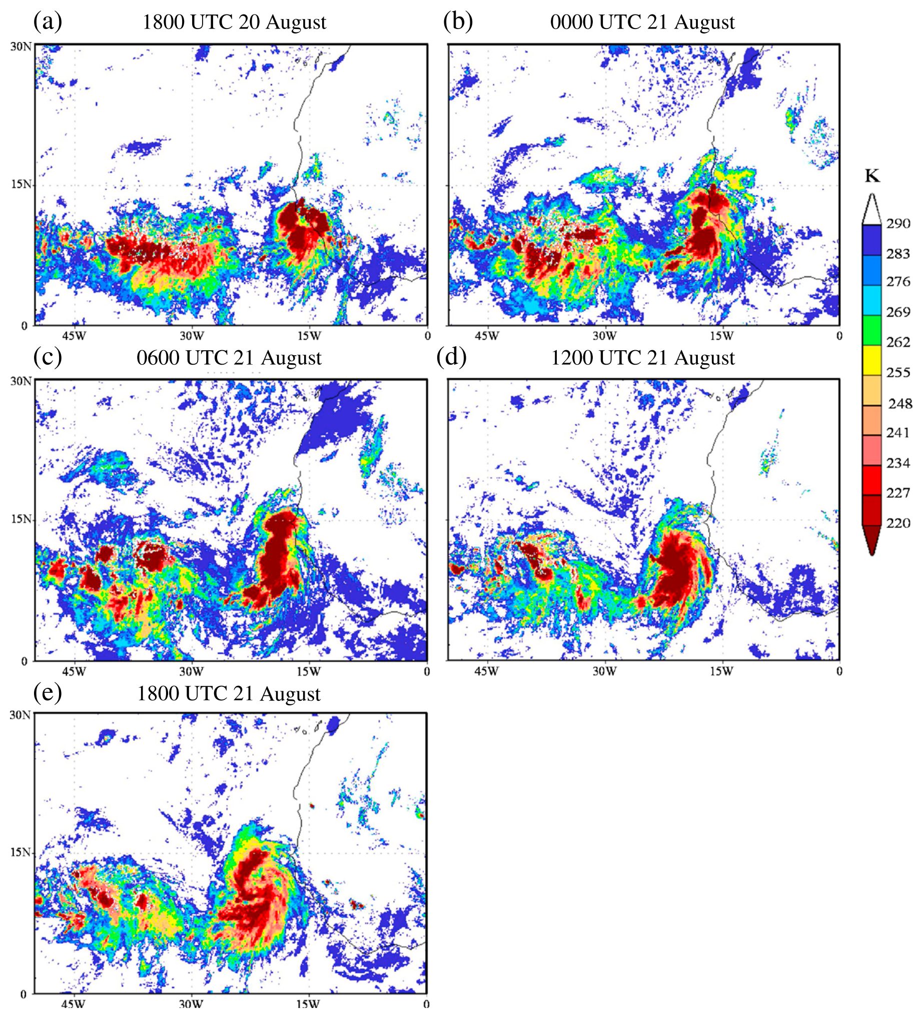

Figure 2. Satellite cloud top brightness temperature retrieval (K) at (a) 1800 UTC on 20 August, (b) 0000 UTC on 21 August, (c) 0600 UTC on 21 August, (d) 1200 UTC on 21 August, and (e) 1800 UTC on 21 August 2006.

2.2. The D-Vortex Merger Process

The D-vortex merger process is demonstrated using the 900 hPa relative vorticity derived from ERAI reanalysis data (Figure 1). Debby's precursor was an African tropical wave, which was accompanied by a wet vortex (W in Figure 1a) and vigorous convective clouds (Figure 2). A D-vortex (D in Figure 1) was found immediately north of both the AEJ and the wet vortex. These two vortices started moving counterclockwise about a point roughly halfway between the two and approaching each other at 1800 UTC on 20 August (Figures 1a and 1b). The wet vortex intensified at 0000 UTC on 21 August but split into two weaker vortices upon leaving the African continent at 0600 UTC on 21 August (W1 and W2 in Figure 1c). Of these two wet vortices, the westernmost vortex (W1 in Figure 1c) merged with the D-vortex at 1800 UTC on 21 August (Figure 1d), the same time that Debby was first classified as a tropical depression. Note that the near-simultaneous occurrence of the D-vortex merger and Debby's classification as a tropical depression does not necessarily imply that Debby's genesis was directly related to the D-vortex merger. Favorable large-scale environmental conditions may have also played a role in Debby's genesis, but more investigation is required to determine the true cause. After the merging process, the vortex became broader and weaker in the early stages of development, then gradually concentrated and intensified again later on (Figures 1e and 1f).

When a dry and a wet vortex merge, there are two possible competing effects. First, the D-vortex merger may increase the low-level vorticity and deepen the wet vortex after ageostrophic wind adjustment, increasing the likelihood of TC genesis. Second, since the D-vortex is warm and dry, its merging with a wet vortex may

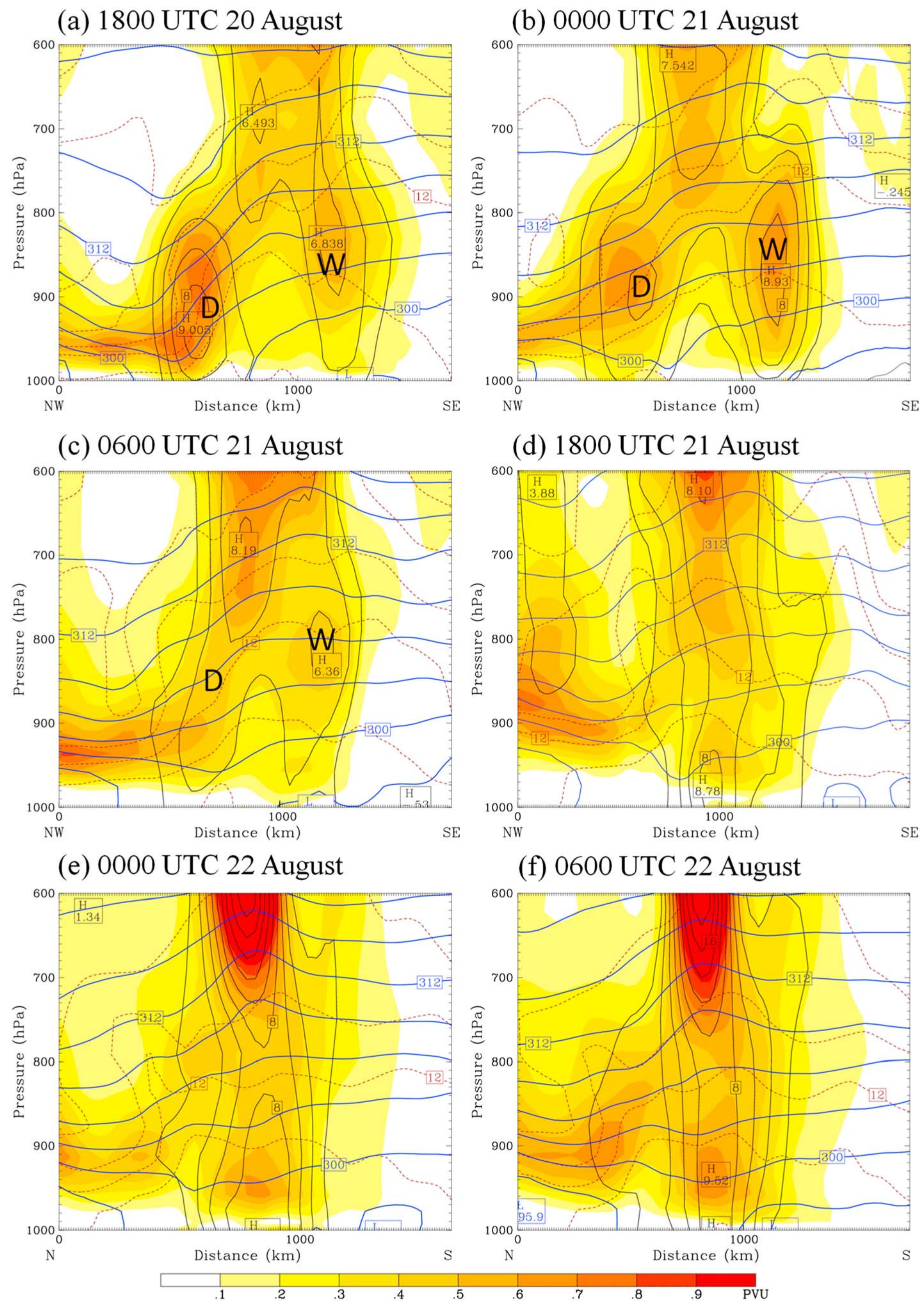

Figure 3. Vertical cross sections of potential vorticity (shading, potential vorticity unit (PVU)), positive relative vorticity (black contour lines, 10^{-5} s^{-1}), potential temperature (blue contour lines, K), and water vapor mixing ratio (brown dotted lines, g kg^{-1}) at (a) 1800 UTC on 20, (b) 0000 UTC on 21, (c) 0600 UTC on 21, (d) 1800 UTC on 21, (e) 0000 UTC on 22, and (f) 0600 UTC on 22 August 2006 along the magenta lines in Figures 1a to 1f, respectively, from the ERAI data. Letters W and D indicate the wet vortex and the D-vortex, respectively.

suppress storm development by reducing relative humidity due to mixing and inducing evaporative cooling, which can generate downdrafts. A quantitative analysis of these counteracting processes would require high-resolution numerical simulations, which are beyond the scope of this study. Nevertheless, a preliminary qualitative analysis was carried out using reanalysis potential vorticity (PV) and moisture fields to gain further insight into the D-vortex merger process.

Vertical cross sections of PV through the 900 hPa relative vorticity maxima of both vortices were produced and analyzed (Figure 3). The shallow D-vortex (D in Figure 3a) was situated near the West African coast and confined

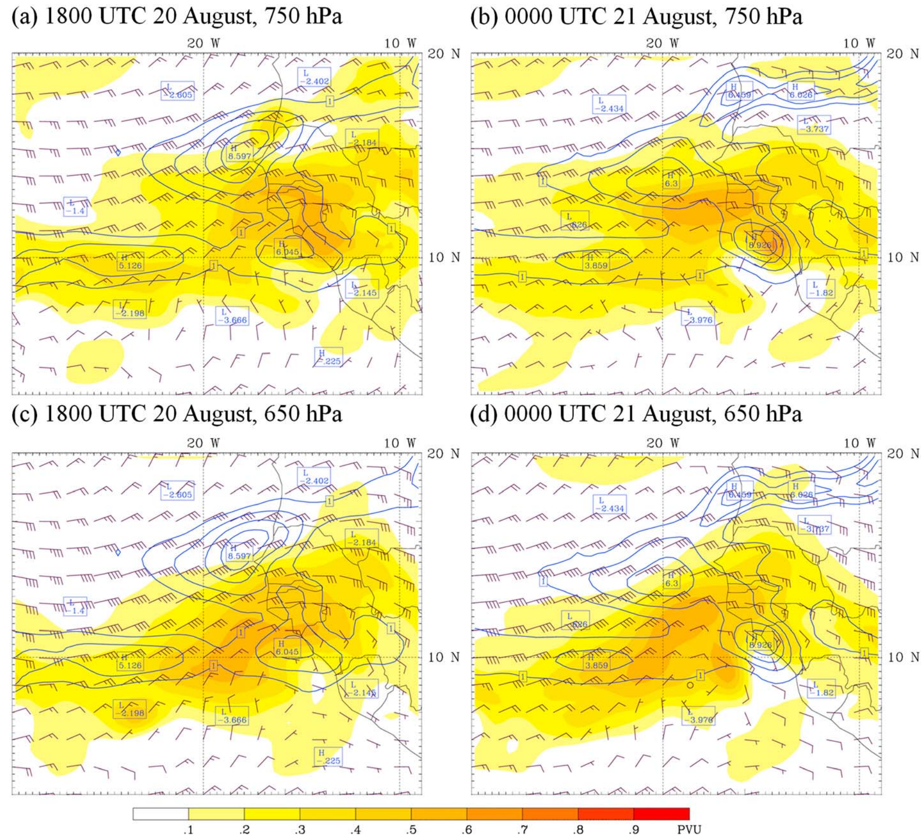

Figure 4. Horizontal cross sections of potential vorticity (shading, PVU) and wind vectors at (a and b) 750 hPa and (c and d) 650 hPa. Figures 4a and 4c are at 1800 UTC on 20 August and Figures 4b and 4d are at 0000 UTC on 21 August. The blue contour lines are 900 hPa positive relative vorticity (10^{-5} s^{-1}) for vortex-position reference.

below the 750 hPa pressure surface at the southern edge of warm (blue solid contours) and dry (brown dotted lines) Saharan air, as indicated by the Saharan air parameter (Figure 1). When this D-vortex moved over the Atlantic at 1800 UTC on 20 August, its PV was greater than that of the wet vortex (W in Figure 3a). The warm D-vortex ascended along with the Saharan air layer, a warm and dry air layer, after moving southwestward over the cooler marine boundary layer. At 0000 UTC on 21 August the PV of the wet vortex increased slightly, possibly due to the vertical gradient of diabatic heating induced by strong convection [*Conzemius and Montgomery*, 2009; *Hsieh and Cook*, 2008], as suggested by the fact that the wet vortex was in phase with the convective moisture tower in Figure 3b. Within the MCS, the vertical gradient of the diabatic heating below the level of the maximum condensational latent heat release tends to stretch the air column. The stretching of the air column consequently increases potential vorticity, assuming that the absolute vorticity is positive, in order to conserve angular momentum. A detailed discussion of the convective generation of PV due to the vertical gradient of diabatic heating and the corresponding equation (3) can be found in *Hsieh and Cook* [2008].

At 750 hPa a local PV maximum positioned itself above the two low-level vortices at 0000 UTC 21 August (Figure 3b). By examining horizontal cross sections of the PV field at different pressure surfaces, we found that at 1800 UTC on 20 August, the 750 hPa PV maximum near the coast still lagged slightly behind the two low-level vortices (Figure 4a), while the PV maximum at 650 hPa was positioned ahead of these vortices (Figure 4c). At 0000 UTC on 21 August the 750 hPa PV maximum propagated westward and caught up to the two low-level vortices (Figure 4b), which was also evident in the vertical cross section in Figure 3b. The 750 hPa PV maximum was also closer to the 650 hPa PV maximum at this time (Figure 4d) than it was previously. Both the 750 hPa and 650 hPa vortices associated with the midlevel AEW remained near the low-level vortices thereafter, supporting a strong midlevel forcing for the merger process that occurred later.

From 0000 UTC to 0600 UTC on 21 August the PV values of both vortices decreased and the D-vortex became linked to the lower portion of the 750 hPa PV maximum. During this time, as mentioned previously, the wet

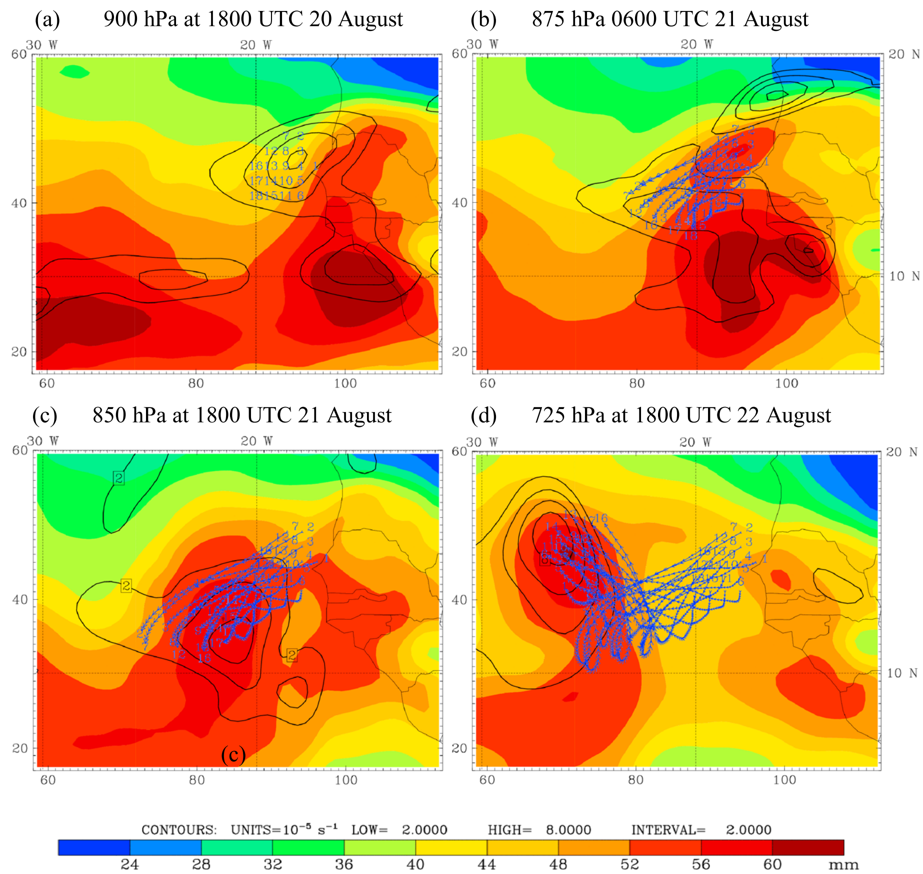

Figure 5. Column integral of water vapor (shading, mm), positive relative vorticity (black contour lines, $10^{-5}\ s^{-1}$) at different pressure levels, and 18 air parcel trajectories (blue arrows with numbers) for (a) 900 hPa at 1800 UTC on 20 August, (b) 875 hPa at 0600 UTC on 21 August, (c) 850 hPa at 1800 UTC on 21 August, and (d) 725 hPa at 1800 UTC on 22 August 2006 from the ERAI data. The 18 trajectories started from 900 hPa within the dry vortex at 1800 UTC on 20 August, the time when the two vortices started merging, and ended at the time of each figure. The plotting level of vorticity for each figure was estimated according to the average height (pressure) of the 18 trajectories at the time of each figure, shown in Figure 6.

vortex split into two vortices (Figure 1c), with the PV maximum of the westernmost vortex shifted out of phase with its associated convective moisture tower (Figure 3c).

After the D-vortex merger at 1800 UTC on 21 August, the merged vortex experienced a slight decrease in PV and a simultaneous increase in overall area (Figure 3d). At the same time, the merged vortex became attached to the lower portion of the 750 hPa PV maximum, extending midlevel PV downward. The merged system did not become vertically coherent until after an ageostrophic wind adjustment 12 h later (Figures 3e and 3f), indicated by the vertical alignment of relative vorticity (black contours). Thereafter, the PV maximum of the merged vortex gradually intensified and realigned itself with the moisture field.

The MCS associated with the wet vortex was still organized after it left the African continent but became broader and weaker soon after the D-vortex merger occurred at 1800 UTC on 21 August (Figure 2). The cloud top brightness temperature showed that the MCS gradually reorganized afterward, as made evident by the coverage of cold brightness temperatures <241 K, but the convection never returned to its original, premerger strength (figure not shown). Consistent with this finding, column-integrated water vapor within the wet vortex decreased following the completion of the merger (Figure 5).

After an ageostrophic wind adjustment, the vortex reorganized and started intensifying. A number of factors were possibly responsible for the intensification, including the D-vortex merger, the restrengthening of deep convection as column-integrated water vapor slowly increased and became confined to a smaller area (Figure 5d), and favorable environmental conditions. A similar result was also seen in the National Centers for Environmental Prediction Final (FNL) global analysis data set (figures not shown).

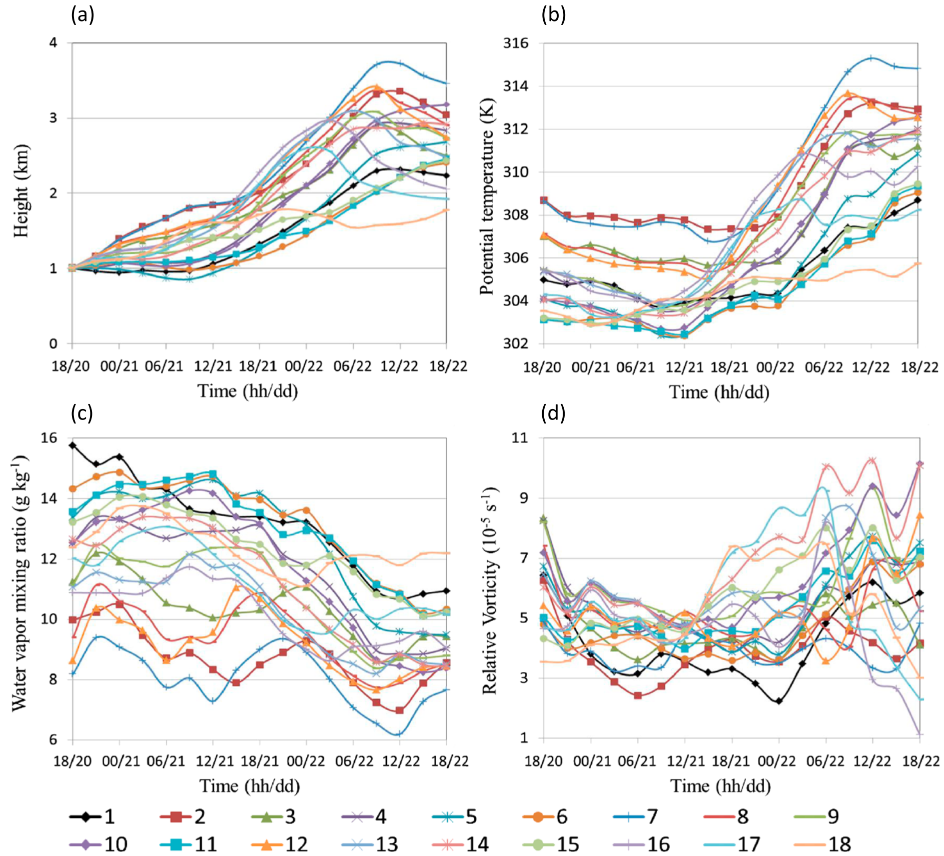

Figure 6. The (a) elevation (km), (b) potential temperature (K), (c) water vapor mixing ratio (g kg^{-1}), and (d) relative vorticity (10^{-5} s^{-1}) of the 18 air parcel trajectories from 1800 UTC on 20 August to 1800 UTC on 22 August 2006. The *x* axis indicates time, where hh is the hour in Zulu (Z) and dd is the date (from 20 to 22 August).

2.3. Forward Trajectory Analysis

To further examine the D-vortex merger process, the forward trajectories of 18 air parcels (blue arrows in Figure 5), initially placed within the D-vortex on the 900 hPa pressure level, were calculated using the ERAI data set, which was temporally interpolated to hourly intervals for the calculation. The air parcels were tracked from 1800 UTC on 20 August, when the two vortices started approaching each other, until 1800 UTC on 22 August.

The results show that during the first half of the tracking period, the warm, dry parcels gradually moved upward from the 900 hPa pressure surface (Figure 6a). At the same time, they experienced slight decreases in potential temperature and relatively large variations in moisture content (Figures 6b and 6c). At 1800 UTC on 21 August, most of the parcels reached the wet vortex after approaching it from the north and northwest (Figure 5c), signaling the occurrence of the D-vortex merger. As these warm, dry parcels moved with the merged vortex, they continued moving upward. It is notable that most of these parcels ascended a bit more rapidly after the vortex merger (Figure 6a), possibly due to the upward motion within the accompanying MCS. During the upward motion from 1800 UTC 21 to 0600 UTC on 22 August, most parcels experienced an increase in potential temperature and a decrease in water vapor mixing ratio (Figures 6b and 6c). Since the ascending dry parcels remained unsaturated during this time, it is likely that these temperature and moisture changes were due to the mixing of warmer and drier environmental air into the parcels. At 0000 UTC on 22 August, parcel number 17, which was close to the center of the storm after the merger (Figure 5c), started to descend. Many other parcels followed suit, and the number of descending parcels reached a maximum at 1200 UTC on 22 August, 18 h after the D-vortex merger. Parcel descent occurred due to a loss of buoyancy as dry air parcels were entrained into convective clouds, which at the time could be found along the east and west sides of the storm (figure not shown), and experienced evaporative cooling. The impact of this process

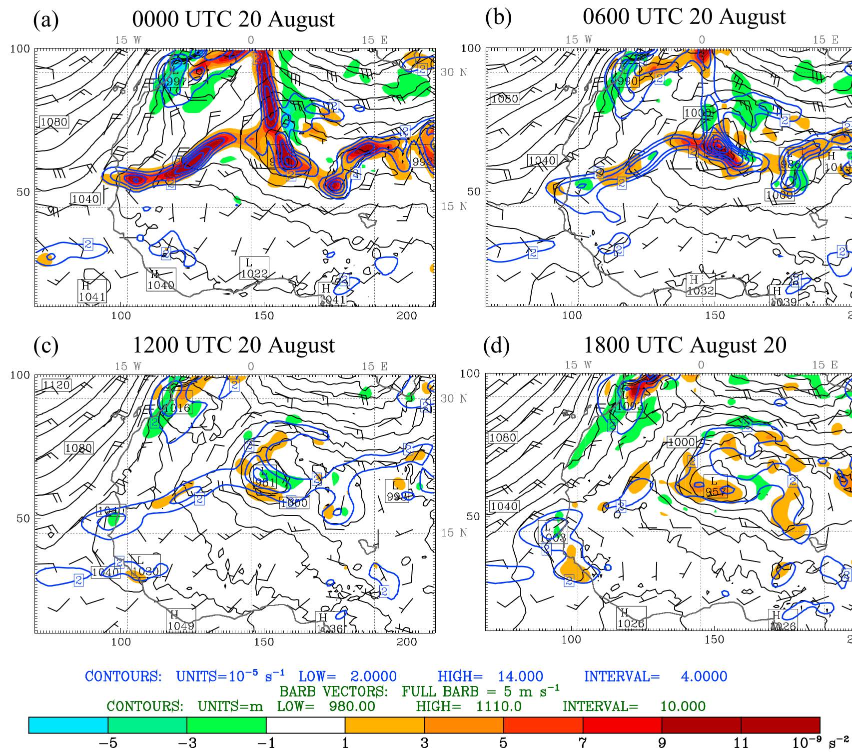

Figure 7. The divergence forcing (shading, 10^{-9} s^{-2}) from the vorticity equation, positive relative vorticity (blue contour lines, 10^{-5} s^{-1}), geopotential height (black contour lines, m), and wind vectors at 900 hPa at (a) 0000 UTC, (b) 0600 UTC, (c) 1200 UTC, and (d) 1800 UTC on 20 August 2006 from the ERAI data.

was revealed by the cooling and moistening of a few parcels near the end of the tracking period and was particularly noticeable for drier parcels, i.e., # 2, 7, 8, and 12 (Figures 5a and 6c).

With regards to relative vorticity (Figure 6d), all but one parcel experienced a decrease at the beginning of the tracking period and remained approximately constant before the D-vortex merger. After the merger at 1800 UTC on 21 August, more than half of the parcels experienced an increase in relative vorticity, a product of the D-vortex merger, while about a third of them saw a decrease or little change at all.

An important question arises from our discussion thus far: how did Debby's predepression vortex survive an infusion of dry air from the Sahara desert? First, it is possible that the vortex merger intensified and organized the preexisting convective vortex to the extent that it was able to persist despite the suppressive effects of dry air within the D-vortex. Second, it is also possible that the wet vortex was initially intense enough to resist the dissipative effects of dry air [*Sippel et al.*, 2011]. In the first scenario, the vortex merger would have been absolutely necessary for Debby's survival and could be a reason why its genesis occurred so rapidly. In the second, however, the storm would have been driven solely by favorable environmental conditions, and the vortex merger would have only hampered Debby's development. As stated earlier, a more thorough examination of the processes involved in the D-vortex merger, including cloud evaporation, requires high temporal and spatial resolution data from a mesoscale model.

3. The Sources of Dry Vortices

Elongated, semipermanent, low-level cyclonic vorticity strips exist throughout northwestern Africa. These vorticity strips develop along the monsoon convergence shearline and within the Saharan desert from midnight (using Debby as an example, Figure 7a) through the early morning (Figure 7b). In general, these vorticity strips become weaker during the day (Figure 7c) due to mixing as the boundary layer deepens and eventually dissolve into individual vortices in the late afternoon (Figure 7d), resulting in a strong diurnal cycle of dry vortex generation. Using ERAI data, analysis of the forcing terms in the vorticity equation, including relative and planetary vorticity advection, divergence, tilting, and baroclinicity, shows that divergence is the dominant mechanism responsible for strengthening these vorticity strips at night (shading in Figure 7). The forcing is due to horizontal wind shear associated with low-level convergence and is maximized at night when winds within the desert become stronger and supergeostrophic [*Stull*, 1988].

A north-northeasterly low-level jet near the West African coast, induced by the interaction of the subtropical high over the eastern Atlantic Ocean and the Saharan heat low, frequently enhances an east-northeast to west-southwest oriented vorticity strip in northwestern Africa (Figure 7a). Vortices that break away or shed from this vorticity strip are a source of dry vortices.

Dry vortices are also produced by low-level lows (African easterly waves) that form in eastern Africa and occasionally the Sahara desert, propagating westward along the intertropical discontinuity (ITD) to the West African coast [*Karam et al*., 2009]. These lows can serve not only as dry vortices but can also merge with and enhance existing dry vortices when leaving the coast. Previous studies have shown that these vortices, which form north of the AEJ, arise due to baroclinic instabilities [*Reed et al*., 1977] and are the northern vortices referenced in *Pytharoulis and Thorncroft* [1999]. The dry vortices typically remain near 20°N during the hurricane season but occasionally move southward (additional discussion in section 4.5). A D-vortex merger is likely if a dry vortex moves southward and reaches southwest Mauritania just as a wet vortex embedded in an African tropical wave south of the AEJ nears the West African coast. TC genesis may follow if the large-scale conditions are favorable. A dry vortex typically lasts for 1–2 days, but sometimes longer, and can merge with a wet vortex after leaving the continent.

4. Statistics: Characteristics of D-Vortex Merger, African Tropical Waves, and the Environment

4.1. Case Selection

The relation between the D-vortex merger and TC genesis over the Atlantic Ocean was investigated for TCs forming between 1980 and 2012. To enhance the robustness of our conclusions, this study examined both developing and nondeveloping systems. Developing systems are defined as North Atlantic storms that originated as African tropical waves and became tropical depressions within the main development region, 6–20°N and 17–60°W, according to the best track data set from National Hurricane Center [*Sabbatelli and Mann*, 2007]. To avoid analyses that are biased by relatively fewer developing systems in July and October, only developing and nondeveloping systems that occurred in August and September were considered in this study. A total of 123 developing systems were identified in August and September over 33 years of data. Storms that became tropical depressions west of 60°W were excluded due to the increased uncertainty involved in tracing these disturbances back to the West African coast.

A nondeveloping system is defined as a tropical wave, originating over Africa and remaining south of the AEJ when leaving the continent, which either did not develop into a tropical depression during its lifetime or became a tropical depression after moving west of 60°W. Of the nondeveloping systems identified in this study, the weakest with no possibility of developing into a tropical depression were singled out and eliminated from consideration using the following criteria. First, we only considered those that formed in August and September, whose averaged 850 hPa relative vorticity between 5°N and 15°N reached a minimum of $0.5 \times 10^{-5}\ s^{-1}$ when leaving the West African coast. Second, since *Peng et al*. [2012] found that 700 hPa relative vorticity is important to cyclogenesis over the eastern Atlantic Ocean, nondeveloping systems were selected only if they were associated with 700 hPa AEWs upon reaching the West African coast. Lastly, since the D-vortex merger is the primary focus of this investigation, if a wet vortex embedded in an African tropical wave reached the West African coast without an accompanying dry vortex north of the AEJ, it was excluded. This final condition eliminated only a few wet vortices from consideration, implying that most wet vortices were accompanied by dry vortices. A total of 269 nondeveloping systems during the 33 year period of interest satisfied all of the above criteria.

4.2. Methodology

Prior to analyzing our data, the 392 selected cases, which included 123 developing systems and 269 nondeveloping systems, were divided into four groups (Table 1): developing systems with a D-vortex merger (DM), developing systems without a D-vortex merger (DN), nondeveloping systems with a D-vortex merger

10.1002/2014JD021749

Table 1. Four Types of African Tropical Disturbances and the Corresponding Number of Cases Identified From August to September During 1980 to 2012

Type	Developing System	Nondeveloping System
D-vortex Merger	86 (DM)	149 (NM)
No D-vortex merger	37 (DN)	120 (NN)

(NM), and nondeveloping systems without a D-vortex merger (NN). The first letter indicates a developing (D) or nondeveloping system (N), while the second letter indicates the merger (M) or nonmerger (N) process. Because it was difficult to track the targeted vortices on an isentropic PV field (figure not shown), we used 900 hPa relative vorticity field to examine the D-vortex merger process, as we did in section 2.

Some nondeveloping systems can undergo a D-vortex merger far from the West African coast. These systems are often difficult to identify because their vortices, in general, are weak and unorganized. Therefore, only those nondeveloping systems whose D-vortex merger occurred before reaching 45°W were counted toward the NM group, while the rest were assigned to the NN group. When the four groups were compared, composite fields from their case members were used for analysis. The statistical significance for different variables was calculated using a Student's two-tailed *t* test or a chi-square test. Note that wind vector differences were considered significant only if both the zonal and meridional wind components pass the 95% confidence level.

The distance between each pair of dry and wet vortices as well as the intensity and relative humidity of both vortices were compared. For most of the vortex pairs, the dry vortex left the West African coast at approximately the same time as the wet vortex. As mentioned in section 3, the production of dry vortices along the ITD and within the Saharan desert is characterized by a strong diurnal cycle due to strong boundary layer mixing during the day. In contrast, the diurnal cycle governing the production of scattered wet vortices south of the AEJ is much weaker. To reduce the influence of this land-based diurnal signal on the intensity of the dry vortices, for each case we selected ERAI data at the first available time after the dry vortex exited the West African coast, rather than the time at which the wet vortex left the coast. For 2.3% of cases, however, we used reanalysis data at the time before the dry vortices left the continent because, in these cases, the wet vortices left the coast much earlier than the dry vortices. This was done only to reduce possible errors in dry-wet vortex distance comparisons introduced by these three cases since paired vortices were seen to approach each other more rapidly after both moved over the ocean, where surface friction was reduced.

The position of an individual vortex was defined as the location of its 900 hPa relative vorticity maximum. The vorticity intensity and relative humidity of each vortex, however, were estimated by averaging values within a cube with three grid points on each side (27-point average) centered on the location of maximum relative vorticity.

4.3. D-Vortex Merger and African Tropical Waves

Analysis showed that 86 of 123 developing systems (~70%) and 149 of 269 nondeveloping systems (55%) considered in this study were associated with a D-vortex merger (Table 1). The question to ask here is, "are the developing systems over the main development region in August and September and the D-vortex merger associated?" We use a chi-square test to examine the null hypothesis of no association between Atlantic developing systems and the D-vortex merger. The chi-square statistic is 7.42, and the P value is 0.0065, which rejected the null hypothesis at a significance level of 0.05. This suggests that there were a statistically significant relation between the Atlantic developing systems and the D-vortex merger, significant at the 95% confidence level.

The composite 900 hPa relative vorticity, wind, and sea level pressure fields for developing systems with and without a D-vortex merger (DM and DN, respectively) were quite similar, but some discrepancies existed nonetheless (Figure 8a versus 8b). Compared to DN, the composite sea level pressure from DM shows a low extending southwestward to the coast, located at about 18–19°N and 15°W. Although the composite positions of dry and wet vortex centers from DM and DN appeared similar in Figure 8, numerical calculation of these positions in standard latitude/longitude coordinates was quantitatively different. The DM dry vortices (i.e., D-vortices) were located to the south of the DN dry vortices, while the DM wet vortices were located to the northwest of the DN wet vortices, resulting in a shorter average distance between the two vortices for the DM cases (992 km for DM versus 1169 km for DN; see Table 2). The shorter average distance between the two

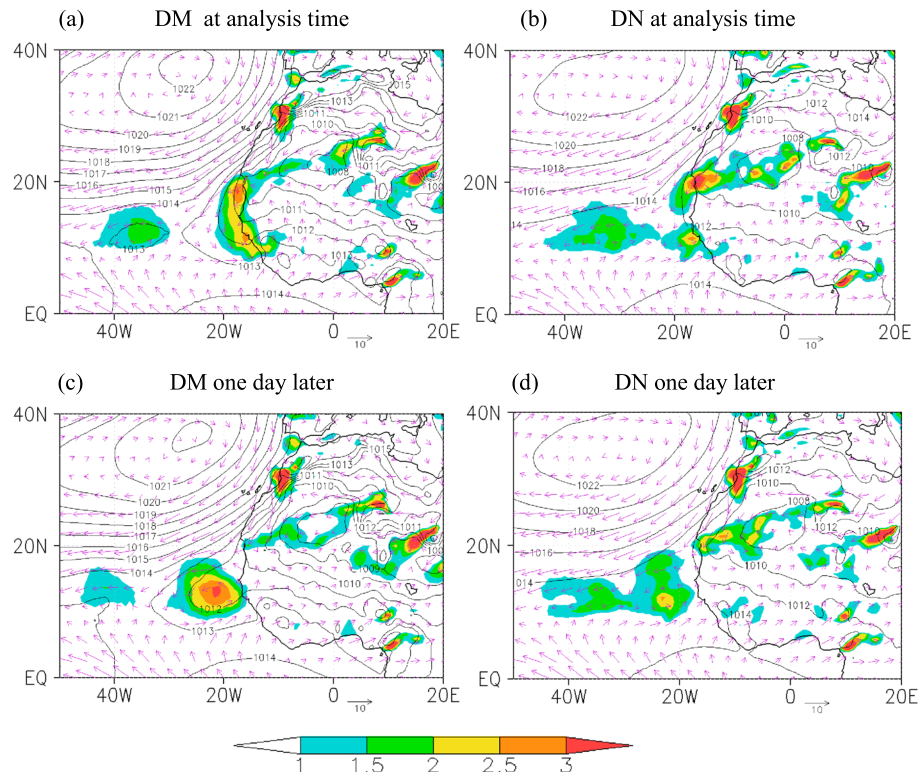

Figure 8. The composite sea level pressure (hPa, black contours), 900 hPa positive relative vorticity ($10^{-5}\ s^{-1}$, shading), and 900 hPa wind vectors for (a) DM (86 cases) and (b) DN (37 cases) at the times when the dry vortex left the West African coast. (c and d) The same as Figures 8a and 8b, respectively, except for 1 day later.

vortices in the DM cases favored and likely contributed to the occurrence of the D-vortex merger [*Melander et al.*, 1988]. The average vorticity intensity of the wet vortices, computed using a 27-point average value about the vortex center, was slightly greater than that of the dry vortices for the DM cases ($7.20 \times 10^{-5}\ s^{-1}$ versus $6.82 \times 10^{-5}\ s^{-1}$; see Table 3). For the DN cases, on the other hand, the wet vortices were weaker than the dry vortices ($5.91 \times 10^{-5}\ s^{-1}$ versus $6.66 \times 10^{-5}\ s^{-1}$). In these cases, however, the dry vortices had no direct influence on the development of the wet convective vortices since no D-vortex merger occurred in these cases.

A comparison of the average vorticity intensity of DM and DN vortices showed that wet vortices were stronger for the DM cases upon leaving the West African coast ($7.20 \times 10^{-5}\ s^{-1}$ for DM versus $5.91 \times 10^{-5}\ s^{-1}$ for DN). DM-merged vortices remained more intense 1 day later after drifting farther westward into the eastern tropical Atlantic (Figure 8c versus 8d).

It is interesting to note that after storms left the African coast, the dry vortex strip was still present north of the AEJ (Figures 8c and 8d), even though wet vortices south of the jet were mostly absent due to their 3–5 day cycle [*Carlson*, 1969a, 1969b; *Burpee*, 1974]. This supports the notion that dry vortex strips existed on a

Table 2. The Average Distance of the Vortex Center, the Average Vorticity Intensity Ratio, and the Average Vortex Size Ratio Between the Dry and Wet Vortex for All Cases Within Each Type[a]

	DM	DN	NM	NN
Distance between two vortices (km)	992	1169	980	1065
Vorticity intensity ratio (dry/wet)	1.14	1.64	1.48	1.57
Vortex size ratio (dry/wet)	1.47	1.96	1.55	2.38

[a]The vortex center is identified using the location of the 900 hPa maximum vorticity. For each vortex, the vorticity intensity is defined by the average of $3 \times 3 \times 3$ points (i.e., 27 points) of data in the *x,y,z* direction, centered at the maximum vorticity of the vortex. The size of a vortex is defined by the number of grid points of the 900 hPa relative vorticity $\geq 2.0 \times 10^{-5}\ s^{-1}$ within a domain of 700 × 700 km centered at the location of the maximum 900 hPa vorticity.

Table 3. Average Vorticity Intensity, RH, and Latitude for Dry and Wet Vortices for All Cases Within Each Type[a]

	Vorticity (10^{-5} s^{-1})		RH (%)		Latitude (°N)	
Type	Dry Vortex	Wet Vortex	Dry Vortex	Wet Vortex	Dry Vortex	Wet Vortex
DM	6.82	7.20	41.75	94.73	18.23	10.23
DN	6.66	5.91	37.97	94.11	19.52	9.68
NM	7.10	6.02	42.99	94.45	18.33	10.21
NN	6.39	5.06	37.44	93.89	18.95	9.92

[a]The latitude is identified by the location of the 900 hPa maximum vorticity. For each vortex, the vorticity intensity and relative humidity are defined by the average value of 3 × 3 × 3 points (i.e., 27 points) data in the *x,y,z* direction centered at the maximum vorticity of the vortex.

semipermanent basis in northwestern Africa, which provides dry vortices over the coast by shedding due to strong horizontal shear or by breaking after the deep boundary layer mixed, in addition to westward propagating lows, as discussed in section 3.

Similar to the developing cases, the average distance between the dry and wet vortices was shorter for the NM cases than for the NN cases (Figure 9a versus 9b, and 980 km versus 1065 km in Table 2), which favored the occurrence of the D-vortex merger in the NM cases. However, unlike the DM cases, the average vorticity intensity of the dry vortices was greater than that of the wet vortices in the NM cases (7.10×10^{-5} s^{-1} versus 6.02×10^{-5} s^{-1}, Table 3). The average intensity of the NM systems appearing 1 day later (Figures 9c and 9d) was greater than that of the NN cases and comparable to that of DN systems.

4.4. Vortex Characteristics Between Developing Systems and Nondeveloping Systems

As examined earlier by the chi-square statistic, the Atlantic developing systems in August and September and the D-vortex merger were statistically associated at a 95% confidence level. However, the number of nondeveloping merger systems (NM) was actually greater than that of DM systems (149 versus 86) and

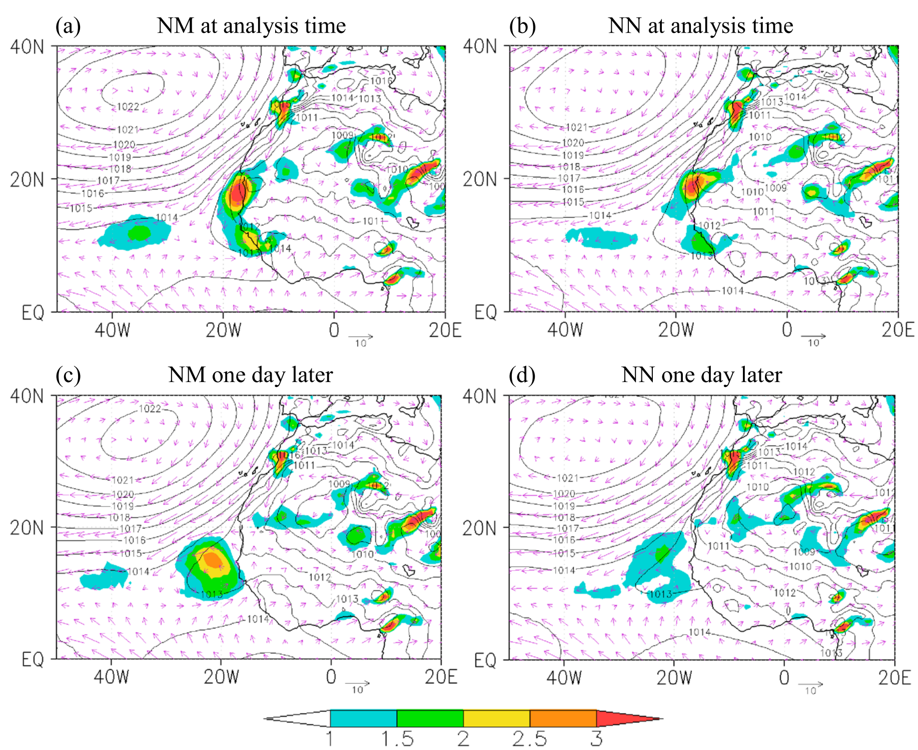

Figure 9. The composite sea level pressure (hPa, black contours), 900 hPa positive relative vorticity (10^{-5} s^{-1}, shading), and 900 hPa wind vectors for (a) NM (149 cases) and (b) NN (120 cases) at the times when the dry vortex left the West African coast. (c and d) The same as Figures 9a and 9b, respectively, except for 1 day later.

Table 4. The Number and Percentage of DM and NM Cases With the Vorticity Intensity Ratio Between the Dry and Wet Vortex (Dry/Wet) <1 and ≥ 1 at the Times When the Dry Vortex Left the West African Coast

Vorticity Intensity Ratio	DM	NM
<1 # (%)	49 (56.98)	57 (38.26)
≥ 1 # (%)	37 (43.02)	92 (61.74)

cannot be ignored. Thus, we turn our attention toward identifying differences between DM and NM cases, starting from the paired vortex characteristics between the two groups.

For each system considered in this study, the vorticity intensity ratio, defined as the ratio of the vorticity intensity of the dry vortex to that of the wet vortex, was calculated (Table 2). The following discussion focuses on the comparison between the DM and NM cases, while DN and NN are mentioned only for reference. The DM cases had an average intensity ratio of 1.14, the smallest among the four groups, and the NM cases had an average value of 1.48. Statistical analysis using a Student's two-tailed *t* test showed that the average intensity ratio of the NM group was significantly larger than that of the DM group at a confidence level of 95%. In addition, the average vorticity intensity of the wet vortices from the DM group was also significantly more intense than that from the NM group, significant at a 95% confidence level.

The DM cases had the highest proportion of systems with intensity ratios less than one (characterized by a stronger wet vortex), at 56.98%, while the NM cases had 38.26% of storms with intensity ratios less than one (Table 4). Another chi-square test was performed to explore if the developing merger systems with D-vortex mergers are statistically associated with a more intense wet vortex and a weaker D-vortex, i.e., the intensity ratio of dry vortex to wet vortex is less than 1 (Table 4). The null hypothesis here is that the developing systems with D-vortex merger are independent to the intensity ratio. The analysis gave a chi-square statistic magnitude of 7.71 and a P value of 0.0055, which rejected the null hypothesis at a significance level of 0.05. This indicates that the developing D-vortex merger systems were statistically associated with a more intense wet vortex and a weaker D-vortex, significant at a 95% confidence level.

In addition to intensity, the average sizes of dry and wet vortices from the DM and NM groups were compared. The size of a vortex was defined by the number of grid points of 900 hPa relative vorticity $\geq 2.0 \times 10^{-5}\,s^{-1}$, the same minimum value shown in Figure 1, within a domain of 700 × 700 km centered at the location of the maximum 900 hPa vorticity. The average of the size ratio of the dry vortex to the wet vortex was 1.47 for DM and 1.55 for NM (Table 2). The size ratio was slightly smaller for DM than for NM, and the difference between the two was not statistically significant using a chi-square test. Compared to DM, the NM cases had significantly weaker wet vortices and average D-vortices were more intense than wet vortices, indicating that the vortex merger tended to hinder the development of the merged vortices in the NM group. This is one possible reason that NM systems failed to develop into TCs even though their average intensity shortly after leaving the continent was similar to that of developing, nonmerging (DN) systems. However, the fact that both DN and NM systems started with comparable intensities but ultimately experienced two vastly different outcomes may also reflect the strong influence of the large-scale environment on TC genesis, in addition to the potential influence of dry air mixing introduced during the D-vortex merger in the NM cases.

The average latitude of the dry and wet vortices immediately after the dry vortices left the coast was calculated (Table 3). When compared to the cases without a D-vortex merger (DN and NN), the wet vortices in both merger cases (DM and NM) were located at a higher average latitude (10.23°N and 10.21°N for DM and NM versus 9.68°N and 9.92°N for DN and NN), while the dry vortices were located at a lower average latitude (18.23°N and 18.33°N for DM and NM versus 19.52°N and 18.95°N for DN and NN). This is consistent with our earlier finding that the distance between dry and wet vortices was shorter for merging systems than for nonmerging systems.

Finally, the average relative humidity of the dry and wet vortices was compared (Table 3). The average relative humidity of the wet vortices was comparable for all four groups, with the highest value appearing for the DM cases (94.73%). As anticipated, the dry vortices were much drier than their southern counterparts. In particular, when compared to merger cases (i.e., DM + NM), dry vortices were drier for the nonmerger cases (DN + NN), likely because, on average, they were located farther north (closer to the desert). Note that while low-level relative humidity did not show much difference between DM and NM, their difference at 500 hPa was large and is discussed in section 4.5.2.

It is worth pointing out that the D-vortex merger usually occurs 1–2 days after vortices leave the West African coast. Thus, the merger process can be detected, and the characteristics of the vortices can be quantified

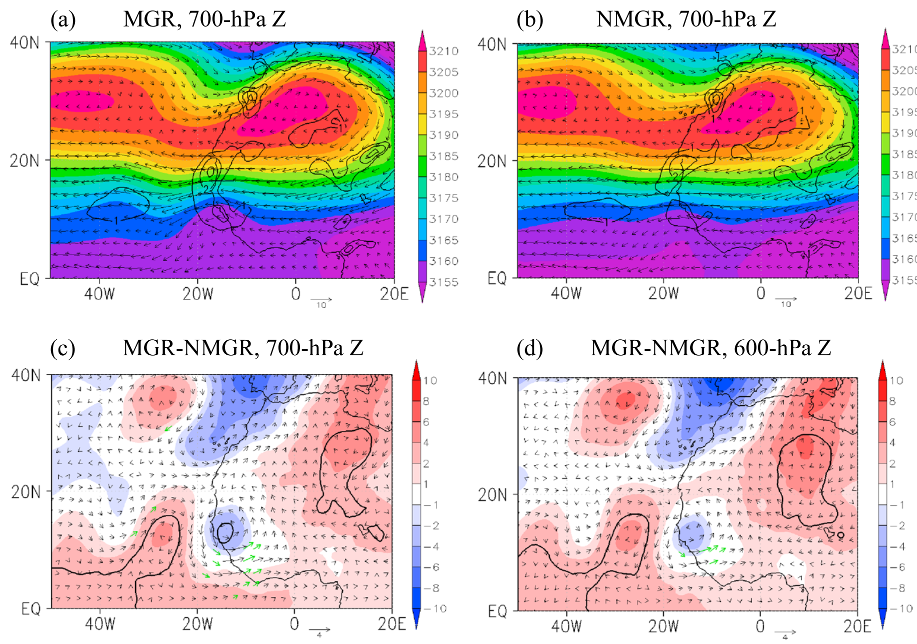

Figure 10. The composite 700 hPa geopotential height (shading, m) and wind vectors and 900 hPa vorticity (contours, $10^{-5}\ s^{-1}$) from (a) the merger cases (DM + NM; MGR), (b) the nonmerger cases (DN + NN; NMGR), and (c) their difference (MGR-NMGR). (d) Same fields as Figure 10c except at 600 hPa. In Figures 10c and 10d, the black thick lines represent the 95% confidence level for the geopotential height difference and the green wind vectors represent the 95% confidence level for the wind difference.

using global analysis data. This means that once the D-vortex merger is identified, the characteristics of vortices could potentially be used to help improve early stage TC genesis forecasting over the eastern Atlantic Ocean.

4.5. D-Vortex Merger and Its Environment Between DM and NM

After identifying the differences in vortex characteristics between the DM and NM cases, it is only natural to examine the role that environmental differences between DM and NM play in creating those vortex differences. However, more than half of the African tropical waves considered in this study were associated with the D-vortex merger after leaving West Africa (70% of developing systems and 55% of nondeveloping systems). Therefore, it seems appropriate to examine how the large-scale environment supports the D-vortex merger by comparing environmental differences between systems with (MGR = DM + NM) and without (NMGR = DN + NN) the D-vortex merger before examining the environmental differences between the DM and NM cases.

4.5.1. Environment Supporting the D-Vortex Merger

Comparison between MGR and NMGR shows that MGR was characterized by more intense 700 hPa AEW activity over the western coast as African tropical waves left the African continent (Figure 10a versus 10b) and manifested as cyclonic circulations in the wind difference field (MGR-NMGR) (Figure 10c). MGR was also characterized by a more intense Saharan high at 30°N over the desert, extending farther eastward, and a higher geopotential height over the ocean crossing the equator to the southwest of West Africa. These two positive geopotential height differences supported the stronger gradient wind circulation associated with the more intense AEW (Figure 10c). All these different characteristics between DM and NM were significant at a 95% confidence level. In MGR, the trough embedded in the westerly to the north of the Saharan air layer was more intense and tilted farther in the northeast-southwest direction, producing a dipole pattern of geopotential height differences over 0–40°W and 30°N–40°N. All aforementioned differences were extended from the low levels to 600 hPa (Figure 10d).

Figure 11 shows the 850 hPa temperature and 900 hPa relative humidity for MGR and NMGR. Compared to NMGR, a warmer temperature difference for MGR occurred over the northern desert, having the maximum at

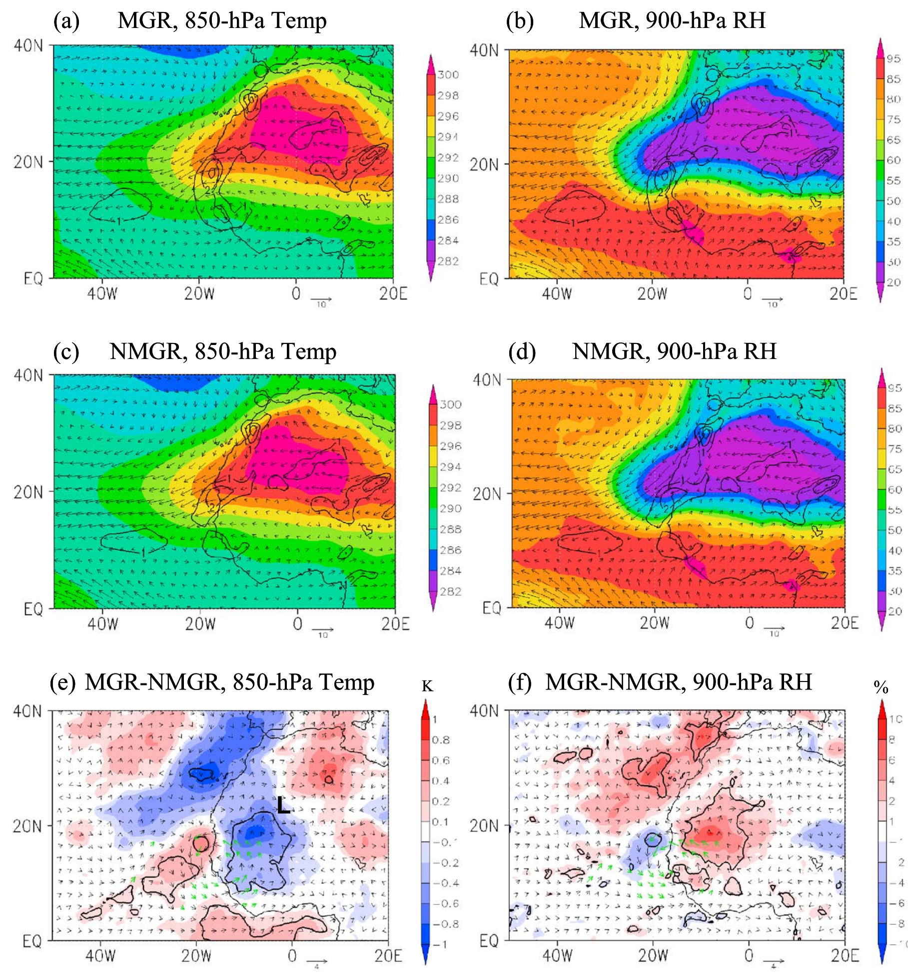

Figure 11. The composite 850 hPa temperature (shading, K) and wind vectors and 900 hPa vorticity (10^{-5} s^{-1}, contours) from (a) the merger cases (MGR), (c) the nonmerger cases (NMGR), and (e) their difference (MGR-NMGR) at the times when the dry vortex left the West African coast. (b, d, and f) The same as Figures 11a, 11c, and 11e, respectively, except for 900 hPa relative humidity (%). The letter L in Figure 11e indicates the location of Saharan low. In Figures 11e and 11f, the thick black lines represent the 95% confidence level for the shaded fields and the green wind vectors represent the 95% confidence level for the wind difference.

5–10°E and 25–30°N, approximately located to the northeast of the Saharan low center. The greater warmth of the Saharan air was relatively shallow (below 700 hPa) and could be attributed in part to higher atmospheric dust amounts over the northern deserts. The absorption of radiation by Saharan dust can increase the temperature of the Saharan air. Although observed aerosol data are not included in the ERAI data, the assimilation of observed temperature indirectly accounts for the aerosol-radiation interaction in the atmosphere. Since there are no direct measurements of the dust-radiative impact on temperature, we examined and compared aerosol optical depth (AOD) retrievals at 0.55 μm from the Moderate Resolution Imagining Spectroradiometer (MODIS) instrument for both MGR and NMGR cases. Note that AOD data were used for only 13 years, after 2000 when they became available, while ERAI includes 33 years. Indeed, AODs were higher for MGR than for NMGR over a similar region, though the differences were not statistically significant (Figure 12). The warmer temperature difference over the northern desert could increase the meridional temperature gradient, which in turn could increase the vertical shear and AEJ strength.

Over southwestern Africa, MGR was significantly colder and more humid than NMGR (Figures 11e and 11f). This is partially due to a greater influx of cool, moist marine boundary layer air into the continental interior of southwestern Africa, triggered by a stronger cyclonic circulation along the West African coast. Cooler temperatures south of the AEJ further enhanced the meridional temperature gradient, producing a stronger

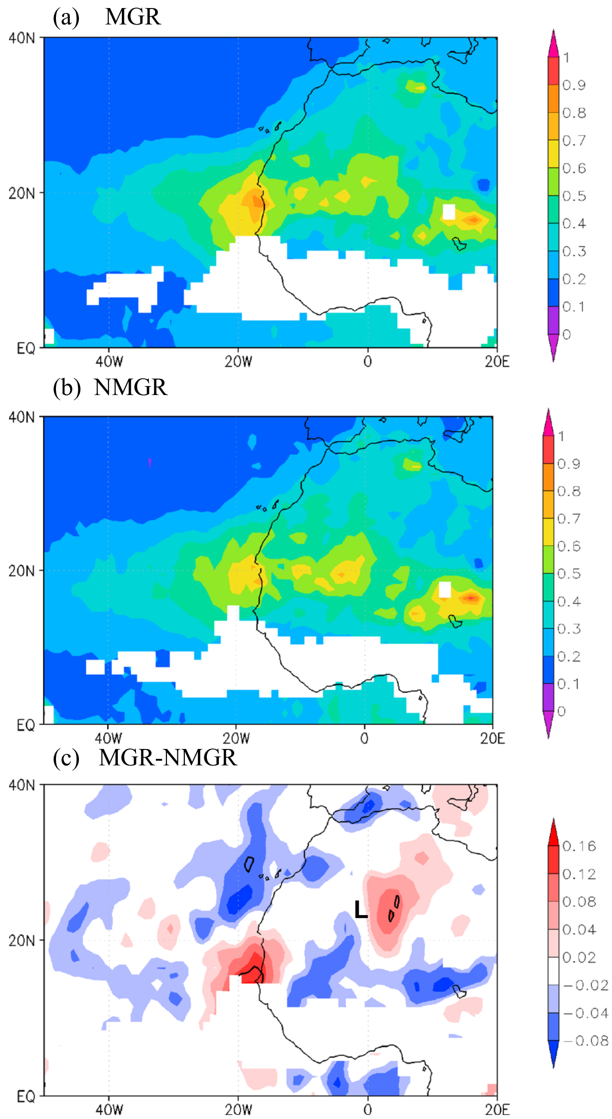

Figure 12. Composite aerosol optical depth (AOD, unitless) from (a) the merger cases (MGR), (b) the nonmerger cases (NMGR), and (c) their difference (MGR-NMGR) when the dry vortex left the West African coast. The thick black lines in Figure 12c represent the 95% confidence level for the shaded field. The letter L in Figure 12c indicates the location of Saharan low. The composite is only calculated when data are available for at least half of the cases. Otherwise, data are considered missing.

AEJ and more intense AEW activity over the coast for MGR (a positive feedback). Note that for MGR, colder temperature and higher relative humidity right outside the northwest African coast was due to the more intense trough imbedded in the westerly at the middle latitudes, which brought cooler air into the region.

In summary, the coastal cyclonic circulation associated with the AEW was more intense for MGR than for NMGR and induced stronger northeasterly winds near the West African coast (Figure 10e). The stronger northeasterly winds were responsible for advecting the warm, dry vortex southwestward, facilitating a D-vortex merger event. The stronger cyclonic circulation and AEW over the coast for MGR were due to the positive geopotential height differences to the northeast and southwest of the AEW, as well as the feedback of the cool marine air advected into southwestern Africa.

4.5.2. Environmental Differences Between DM and NM

Environmental conditions for DM and NM were compared by taking their differences. In addition to differences in vortex characteristics (section 4.4), this comparison helped identify key differences between DM from NM, which could potentially be used to improve TC genesis prediction associated with the D-vortex merger. Compared to NM, DM had warmer 900 hPa temperatures over much of the desert and extending to the ocean, significant at a 95% confidence level (Figure 13a). The warm temperature difference was still clearly shown at 700 hPa (Figure 13b), though the coverage of the significant areas was smaller than that at 900 hPa. The warmer air over the Saharan desert and the Atlantic Ocean could increase the meridional temperature gradient and vertical shear over the intertropical discontinuity (ITD) and the African coast, resulting in stronger AEJs and AEWs. The difference in geopotential heights showed a stronger AEJ and AEW for DM (figure not shown). However, the difference did not reach the 95% confidence level. While temperature differences between DM and NM covered a large area of desert, the difference in AOD between DM and NM seemed small and insignificant (figure not shown), indicating that the average suspended dust amounts over the desert between DM and NM were comparable.

A positive 900 hPa relative humidity difference for DM was present over the eastern Atlantic Ocean between 10 and 20°N, along the path of the west-northwestward propagating storms (Figure 14a). At pressure levels higher in the atmosphere, compared to 900 hPa, the magnitude of the positive relative humidity difference increased and the coverage broadened (Figure 14b), significant at a 95% confidence level starting from the 850 hPa level and up. A higher relative humidity from low to middle levels is a favorable condition

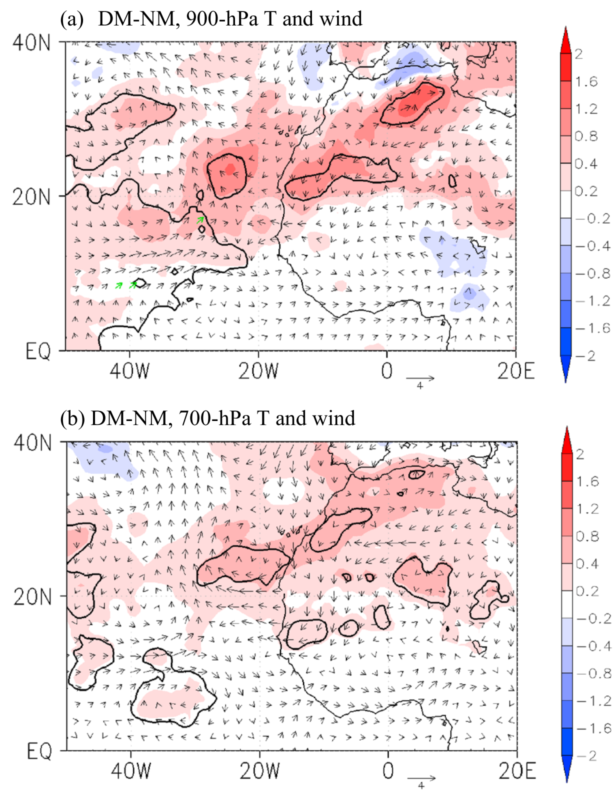

Figure 13. Differences in the composite temperature (shading, K) and wind vectors at (a) 900 hPa and (b) 700 hPa between DM and NM (DM-NM). The thick black lines represent the 95% confidence level for the shaded field. The green wind vectors represent the 95% confidence level for the wind difference.

for TC genesis and has been pointed out previously [*Gray*, 1968]. The maximum positive relative humidity difference between DM and NM was shifted toward the southeast and extended to above the location of the low-level wet vortex (Figure 14c). Over the wet vortex region, the relative humidity difference between DM and NM was small or nil at 900 hPa (Figure 14a), while it was clearly much more significant at 500 hPa (Figure 14c) and above. This implied that wet vortices for DM were often associated with deeper, vigorous convective clouds and could be detected using 500 hPa relative humidity.

The Saharan air parameter (SAP), which indicates the warmth and dryness of the desert air, was compared for DM and NM (Figure 15). In general, a large SAP indicates warmer and drier Saharan air. For both DM and NM, the SAP was greatest in northwestern North Africa (Figures 15a and 15b) and decreased moving away from this region. The contour marking an SAP value of 1 sagged southward along the coastline for both the DM and NM cases, representing the southward propagation of D-vortices. The SAP for DM was greater north of the AEJ near the coast (Figure 15c), which was due to warmer temperature and lower relative humidity over the region (Figures 13a and 14a). The SAP was smaller along 20°N for DM than NM because the air was slightly moister south of the monsoon shearline. The moister air reduced the negative influence of dry air transported southward by the D-vortex merger and was another possible reason why DM systems developed into TCs while NM systems did not.

5. Summary and Conclusions

A vortex merger between a vortex embedded in a convective tropical wave (called a wet vortex) south of the AEJ and a shallow dry vortex (called a D-vortex) north of the AEJ, referred to as a D-vortex merger in this study, was previously identified and linked to several TC cases [e.g., *Ross and Krishnamurti*, 2007]. The goal of this study is to investigate the relation of the D-vortex merger to tropical cyclone (TC) genesis over the Atlantic Ocean based on statistical analysis using the European Centre for Medium-Range Weather Forecasts Re-Analysis Interim (ERAI) data set.

Dry vortices shedding or breaking from the western edge of a vortex strip in northwestern Africa, or originating from westward propagating lows along the intertropical discontinuity, can be advected southwestward and potentially serve as D-vortices in the merging process. Note that a D-vortex is a dry vortex that undergoes the merging process, but not all dry vortices are D-vortices. While the African tropical waves have a frequency of 3–5 days [*Burpee*, 1974], dry vortices are produced at a higher frequency by the low-level semipermanent dry vortex strip over northwest Africa and by westward propagating lows. To better understand the potential role of the D-vortex merger in TC genesis, 33 years of ERAI reanalysis data in the months of August and September were used to investigate the differences between developing (TC) and nondeveloping systems associated with a D-vortex merger. A total of 392 cases (123 developing systems and 269 nondeveloping systems) were selected and divided into four

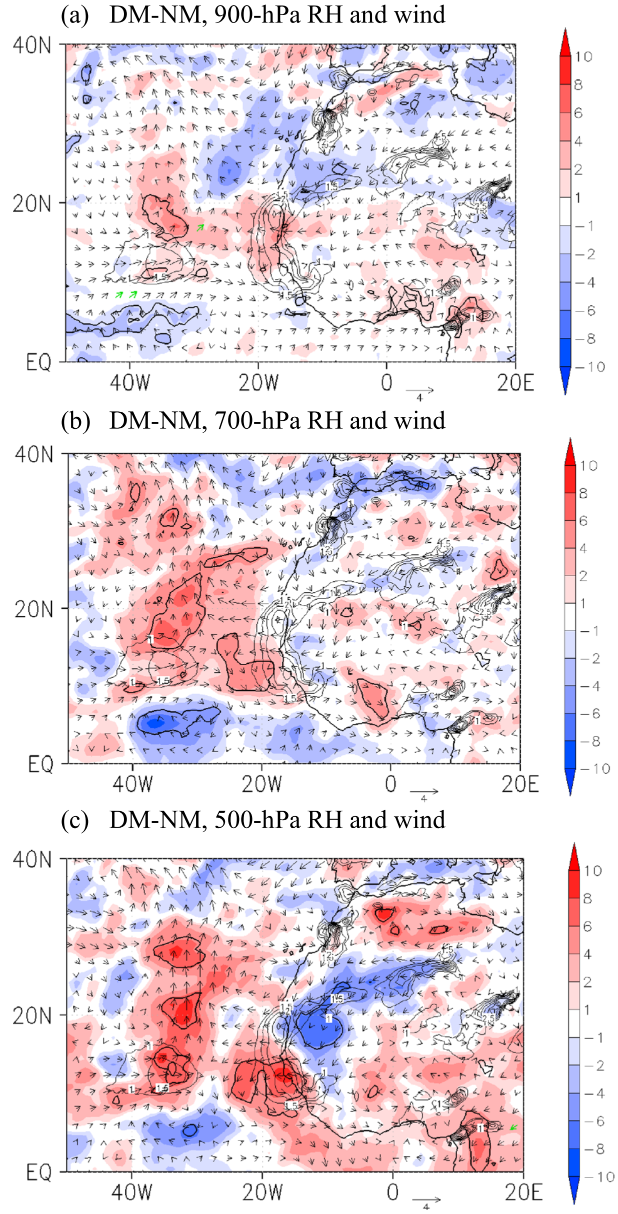

Figure 14. Differences of the composite relative humidity (%) and wind vectors at (a) 900 hPa, (b) 700 hPa, and (c) 500 hPa between DM and NM (DM-NM). The thick black lines represent the 95% confidence level for the shaded field. The green wind vectors represent the 95% confidence level for the wind difference. The thin black contours in Figures 14b and 14c is 900 hPa relative vorticity for DM.

groups for analysis: developing systems with a D-vortex merger (DM), developing systems without a D-vortex merger (DN), nondeveloping systems with a D-vortex merger (NM), and nondeveloping systems without a D-vortex merger (NN). Because we are primarily interested in the potential for the D-vortex merger to serve as a predictor for TC genesis, the analyses are more focused on DM and NM than DN and NN.

Analysis showed that 70% of developing systems were associated with the D-vortex merger over the main development region of the Atlantic Ocean (6–20°N and 17–60°W). However, 55% of nondeveloping systems (NM) were also involved with the process. The chi-square test indicated that the developing systems over the main developing region originating from Africa and the D-vortex merger were correlated, significant at a 95% confidence level.

Analysis showed that the D-vortex merger was modulated by the large-scale conditions, particularly over land. As tropical waves exited the African continent, the AEW over the West African coast was significantly more intense for African tropical waves that underwent a D-vortex merger (MGR = DM + NM) than for those that did not (NMGR = DN + NN). Compared to NMGR, the AEW for MGR was enhanced by two significant, positive geopotential height differences extending from low levels to middle levels; one to the southwest and the other to the northeast of the wave. These induced stronger gradient wind circulations. The stronger cyclonic circulations were partially responsible for driving cool, moist, low-level marine air farther northeastward over the African continent, resulting in cooler temperatures south of the monsoon shearline for MGR, thus strengthening the meridional temperature gradient, the AEJ, and the AEW intensity near the coast. The stronger coastal cyclonic circulations, due to more intense AEWs, produced significantly stronger northeasterly winds along the West African coast, helping to advect the dry vortex southwestward and increase the probability of a D-vortex merger event. Statistical analysis for the environmental differences between DM and NM showed that DM had significantly warmer Saharan air and higher low- to middle-level relative humidity along the storm's path over the eastern Atlantic Ocean, which differentiated DM from NM, in addition to their discrepancies in vortex characteristics.

While the D-vortex merger may increase the likelihood of TC genesis by increasing the intensity and depth of an existing disturbance, it is also possible that developing D-vortex merger (DM) systems could have developed

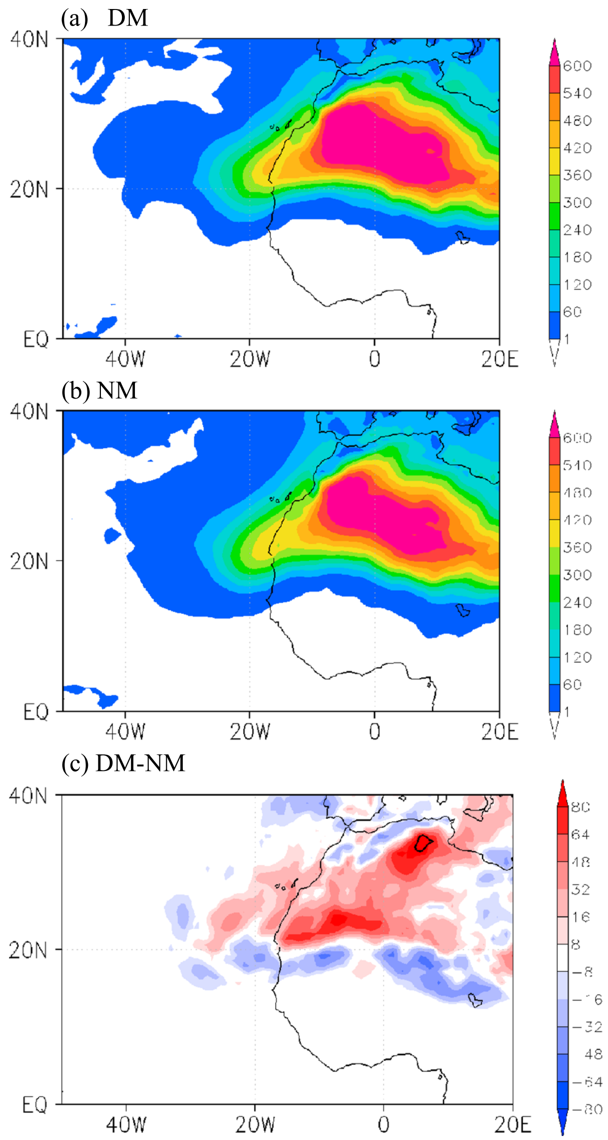

Figure 15. Composite Saharan air parameter (shading, K) from (a) DM, (b) NM, and (c) their difference (DM-NM) when dry vortices left the West African coast. The thick black lines in Figure 15c represent the 95% confidence level for the shaded field.

into tropical depressions without the merger process. If true, the D-vortex merger could simply be a natural response to the strong relative vorticity associated with the convective tropical waves, a shorter distance between the dry and wet vortices, and favorable environment conditions (i.e., stronger Saharan air and AEW). Regardless, our results demonstrated a statistical correlation, instead of a clear causal relation, between the D-vortex merger and TC genesis. The study shows the importance of low-level relative vorticity and low- to middle-level relative humidity, which are commonly used in TC genesis prediction [*Emanuel and Nolan*, 2004; *Singh et al.*, 2014]. However, our statistical analyses have shown other significant differences between DM and NM: (1) the average intensity ratio of the dry vortex to wet vortex was significantly smaller for DM than NM, and the average intensity of the wet vortices was significantly more intense for DM than NM, (2) the 500 hPa relative humidity above the wet vortices was significantly higher for DM than NM, and (3) the low-level Saharan air over the desert was significantly warmer for DM than NM. These three parameters can potentially be used to improve Atlantic TC genesis forecasts over the main development region for cases in which an African tropical wave associated with a D-vortex merger is identified after it moves over the eastern Atlantic Ocean. Of course, when considering the likelihood of TC genesis at any given time, characteristics of the large-scale environment, such as sea surface temperature, low- to middle-level humidity, and vertical wind shear, must also be considered. Finally, the D-vortex merger usually occurs from the West African coast to the eastern Atlantic Ocean. The merger process and the characteristics of the vortices outlined in this study can be detected using analysis data, which can be used in the future to potentially help predict TC genesis in its early stages.

Appendix A: Acronyms That Are Used in This Study

AEJ	African easterly jet.
AEW	African easterly wave.
AOD	aerosol optical depth.
CGI	cyclone genesis index.
DM	developing systems with the D-vortex merger.
DN	developing systems without the D-vortex merger.
EARI	European Centre for Medium-Range Weather Forecasts Re-Analysis Interim.
FNL	National Centers for Environmental Prediction final global analysis data set.

GP	genesis potential.
ITD	intertropical discontinuity.
MCS	mesoscale convective system.
MGR	system with the D-vortex merger.
MODIS	Moderate Resolution Imagining Spectroradiometer.
NASA	National Aeronautics and Space Administration.
NM	nondeveloping systems with the D-vortex merger.
NMGR	system without the D-vortex merger.
NN	nondeveloping systems without the D-vortex merger.
PV	potential vorticity.
RH	relative humidity.
SAP	Saharan air parameter.
TC	tropical cyclone.

Acknowledgments
This work is supported by the NASA Hurricane Science Research Program (grant NNX09AC38G) that is directed by Ramesh Kakar at NASA Headquarters. Yi-Chin Liu is supported by Scientific Discovery through Advanced Computing (SciDAC) program funded by the U.S. Department of Energy (DOE) Office of Advanced Scientific Computing Research and Office of Biological and Environmental Research. The Pacific Northwest National Laboratory (PNNL) is operated for the DOE by Battelle Memorial Institute under contract DE-AC06-76RLO 1830. The data used for this paper include the following: ERAI data produced by European Centre for Medium-Range Weather Forecasts and available at Computational and Information Systems Laboratory/National Center for Atmospheric Research (http://rda.ucar.edu/datasets/ds627.0/); Daily AOD data produced by the Giovanni online data system, developed and maintained by the NASA GES DISC; globally merged (60°N–60°S) pixel-resolution inferred brightness temperature data archived and distributed by the Goddard Earth Sciences (GES) Data and Information Services Center (DISC); and TC best track data obtained from National Hurricane Center (http://www.nhc.noaa.gov/data/). The authors would like to thank Jiun-Dar Chern at NASA/GSFC, Hung-Chi Kuo at National Taiwan University, and Kenneth Earl, Mark Waylonis, and Dustin Grogan at University of California, Davis, for their scientific discussions. The authors would also like to acknowledge Jhih-Ying Chen and Lian-Jie Wang at National Central University in Taiwan and Sabrina Cochrane at the University of California, Davis, for their help in processing data and making some figures.

References

Avila, L. A., R. J. Pasch, and J. Jiing (2000), Atlantic tropical systems of 1996 and 1997: Years of contrast, *Mon. Weather Rev.*, *128*, 3695–3706.

Berry, G., and C. Thorncroft (2005), Case study of an intense African easterly wave, *Mon. Weather Rev.*, *133*, 752–766.

Bruyere, C. L., G. J. Holland, and E. Towler (2012), Investigating the use of a genesis potential index for tropical cyclones in the north Atlantic basin, *J. Clim.*, *25*, 8611–8626, doi:10.1175/JCLI-D-11-00619.1.

Burpee, R. W. (1974), Characteristics of North African easterly waves during the summers of 1968 and 1969, *J. Atmos. Sci.*, *31*, 1556–1570.

Carlson, T. N. (1969a), Synoptic histories of three African disturbances that developed into Atlantic hurricanes, *Mon. Weather Rev.*, *97*, 256–275.

Carlson, T. N. (1969b), Some remarks on African disturbances and their progress over tropical Atlantic, *Mon. Weather Rev.*, *97*, 716–726.

Conzemius, R. J., and M. T. Montgomery (2009), Clarification on the generation of absolute and potential vorticity in mesoscale convective vortices, *Atmos. Chem. Phys.*, *9*, 7591–7605.

Emanuel, K. A. (2010), Tropical cyclone activity downscaled from NOAA-CIRES reanalysis, 1908-1958, *J. Adv. Model. Earth Syst.*, *2*, 1–12, doi:10.3894/JAMES.2010.2.1.

Emanuel, K. A., and D. S. Nolan (2004), Tropical cyclone activity and global climate system, paper presented at 26th Conference on Hurricanes and Tropical Meteorology, Amer. Meteorol. Soc., Miami, Fla.

Gray, W. M. (1968), Global view of the origin of tropical disturbances and storms, *Mon. Weather Rev.*, *96*, 669–700.

Hsieh, J.-S., and K. H. Cook (2008), On the instability of the African easterly jet and the generation of African waves: Reversals of the potential vorticity gradient, *J. Atmos. Sci.*, *65*, 2130–2151.

Jenkins, G. S., A. S. Pratt, and A. Heymsfield (2008), Possible linkages between Saharan dust and tropical cyclone rain band invigoration in the eastern Atlantic during NAMMA-06, *Geophys. Res. Lett.*, *35*, L08815, doi:10.1029/2008GL034072.

Karam, D. B., C. Flamant, P. Tulet, M. C. Todd, J. Pelon, and E. Williams (2009), Dry cyclogenesis and dust mobilization in the inter-tropical discontinuity of the West African monsoon: A case study, *J. Geophys. Res.*, *114*, D05115, doi:10.1029/2008JD010952.

Karyampudi, V. M., and H. F. Pierce (2002), Synoptic-scale influence of the Saharan air layer on tropical cyclogenesis over the eastern Atlantic, *Mon. Weather Rev.*, *130*, 3100–3128.

Landsea, C. W. (1993), A climatology of intense (or major) Atlantic Hurricanes, *Mon. Weather Rev.*, *121*, 1703–1713.

McGauley, M. G., and D. S. Nolan (2011), Measuring environmental favorability for tropical cyclogenesis by statistical analysis of threshold parameters, *J. Clim.*, *24*, 5968–5997.

Melander, M. V., N. J. Zabusky, and J. C. McWilliams (1988), Symmetric vortex merger in two dimensions: Causes and conditions, *J. Fluid Mech.*, *195*, 305–340.

Peng, M. S., B. Fu, T. Li, and D. E. Stevens (2012), Developing versus nondeveloping disturbances for Tropical cyclone formation. Part I: North Atlantic, *Mon. Weather Rev.*, *140*, 1047–1066.

Pytharoulis, I., and C. Thorncroft (1999), The low-level structure of African easterly waves in 1995, *Mon. Weather Rev.*, *127*, 2266–2280.

Reed, R. J., D. C. Norquist, and E. E. Recker (1977), The structure and properties of African wave disturbances as observed during Phase III of GATE, *Mon. Weather Rev.*, *105*, 317–333.

Ross, R. S., and T. N. Krishnamurti (2007), Low-level African easterly wave activity and its relation to Atlantic tropical cyclogenesis in 2001, *Mon. Weather Rev.*, *135*, 3950–3964.

Sabbatelli, T. A., and M. E. Mann (2007), The influence of climate state variables on Atlantic Tropical Cyclone occurrence rates, *J. Geophys. Res.*, *112*, D17114, doi:10.1029/2007JD008385.

Singh, S. K., N. Jaiswal, C. M. Kishtawal, R. Singh, and P. K. Pal (2014), Early detection of cyclogenesis signature using global model products, *IEEE Trans. Geosci. Remote Sens.*, *52*(8), 5116–5121.

Sippel, J. A., S. A. Braun, and C.-L. Shie (2011), Environmental influences on the strength of Tropical Storm Debby (2006), *J. Atmos. Sci.*, *68*, 2557–2581.

Stull, R. B. (1988), *An Introduction to Boundary Layer Meteorology*, 670 pp., Kluwer Acad., Norwell, Mass.

Tippett, M. K., S. J. Camargo, and A. H. Sobel (2011), A Poisson regression index for tropical cyclone genesis and the role of large-scale vorticity in genesis, *J. Clim.*, *24*, 2335–2357.

Ventrice, M. J., C. D. Thorncroft, and M. A. Janiga (2012), Atlantic tropical cyclogenesis: A three-way interaction between an African easterly wave, diurnally varying convection, and a convectively coupled atmospheric Kelvin wave, *Mon. Weather Rev.*, *140*, 1108–1124.

Vizy, E. K., and K. H. Cook (2009), Tropical storm development from African easterly waves in the eastern Atlantic: A comparison of two successive waves using a regional model as part of NASA AMMA 2006, *J. Atmos. Sci.*, *66*, 3313–3334.

Zawislak, J., and E. J. Zipser (2010), Observations of seven African easterly waves in the East Atlantic during 2006, *J. Atmos. Sci.*, *67*, 26–43.

Zipser, E. J., et al. (2009), The Saharan air layer and the fate of African easterly waves—NASA's AMMA field study of tropical cyclogenesis, *Bull. Am. Meteorol. Soc.*, *90*, 1137–1156, doi:10.1175/2009BAMS2728.1.